Climate Subsystems: Pacemakers of Decadal Climate Variability

Anastasios A. Tsonis

Atmospheric Sciences Group, Department of Mathematical Sciences, University of Wisconsin-Milwaukee, Milwaukee, Wisconsin, USA

This paper is a synthesis of work spanning the last 25 years. It is largely based on the use of climate networks to identify climate subsystems and to subsequently study how their collective behavior explains decadal variability. The central point is that a network of coupled nonlinear subsystems may at times synchronize. If during synchronization the coupling between the subsystems increases, the synchronous state may be destroyed, shifting climate to a new regime. This climate shift manifests itself as a change in global temperature trend. This mechanism, which is consistent with the theory of synchronized chaos, appears to be a very robust mechanism of the climate system. It is found in the instrumental records and in forced and unforced climate simulations, as well as in proxy records spanning several centuries.

1. INTRODUCTION

The story in this chapter starts in the mid-1980s when new and exciting approaches to nonlinearly analyze time series "hit the market." At that time, very few in the atmospheric sciences community had heard terminology such as "fractals," "chaos theory," "strange attractors," and the like. A few innovative scientists, however, were experimenting with these new ideas and soon reports of "fractality" and "low dimensionality" in climate records, and other geophysical data begun to surface. These climate records represented dynamics over different time scales ranging from very long (thousands of years) [*Nicolis and Nicolis*, 1984] to very short (hours) [*Tsonis and Elsner*, 1988]. Virtually every report suggested underlying attractors of dimensions between 3 and 8. These early results suggested that climate variability may indeed be described by only a few equations. This resulted in both enthusiasm and hope that climate variability may be tamed after all, and in fierce opposition. Fortunately, this "tug of war" did not eliminate interest in this new theory; rather, it led to a deeper understanding of the nonlinear character of nature and to new insights about the properties of the climate system. This chapter is a small part of what we have learned so far, and it largely draws from my work over the years.

The initial opposition to those dimension estimates seemed to be that in all these studies, the sample size was simply too small. While this issue has been debated extensively [*Smith*, 1988; *Nerenberg and Essex*, 1990; *Tsonis*, 1992, *Tsonis et al.*, 1994], it has not been settled beyond doubts. In a sense, it is naïve to imagine that our climate system (a spatially extended system of infinite dimensional state space) is described by a grand attractor let alone a low-dimensional attractor. If that were the case, then all observables representing different processes should have the same dimension, which is not suggested from the myriad of reported dimensions. *Tsonis and Elsner* [1989] suggested that if low-dimensional attractors exist, they are associated with subsystems each operating at different space and/or time scales. In his study on dimension estimates, *Lorenz* [1991] concurs with the suggestion of *Tsonis and Elsner* [1989]. These subsystems may be nonlinear and exhibit a variety of complex behaviors. All subsystems are connected with each other, as in a web, with various degrees of connectivity. Accordingly, any subsystem may transmit "information" to another subsystem thereby perturbing its behavior. This "information" plays the role of an ever-present external noise, which perturbs the subsystem, and depending on the connectivity of a subsystem to another subsystem, the effect can be dramatic or

Extreme Events and Natural Hazards: The Complexity Perspective
Geophysical Monograph Series 196

10.1029/2011GM001053

negligible. Subsystems with weak connectivities will be approximately "independent," and as such, they may exhibit low-dimensional chaos. It is also possible that the connectivity between subsystems may vary in time, and this effect may dictate the variability of the climate system.

Given the above, the question arises. If subsystems exist in the climate system, what are they and what physics can we infer from them?

2. SEARCHING FOR SUBSYSTEMS

2.1. Methods and Results From Observations

Answers on the nature, geographical basis, and physical mechanisms underlying these subsystems are provided by recent developments in graph theory and networks. Networks relate to the underlying topology of complex systems with many interacting parts. They have found many applications in many fields of sciences. In the interest of completeness, a short introduction to networks is offered next.

A network is a system of interacting agents. In the literature, an agent is called a node. The nodes in a network can be anything. For example, in the network of actors, the nodes are actors that are connected to other actors if they have appeared together in a movie. In a network of species, the nodes are species that are connected to other species they interact with. In the network of scientists, the nodes are scientists that are connected to other scientists if they have collaborated. In the grand network of humans, each node is an individual, which is connected to people he or she knows. There are four basic types of networks.

2.1.1. Regular (ordered) networks. These networks are networks with a fixed number of nodes, each node having the same number of links connecting it in a specific way to a number of neighboring nodes (Figure 1, left). If each node is linked to all other nodes in the network, then the network is a fully connected network. When the number of links per node is high, regular networks have a high (local) clustering coefficient. In this case, loss of a number of links does not break the network into noncommunicating parts. In this case, the network is stable, which may not be the case for regular networks with small local clustering. Also, unless networks are fully connected, they have a large diameter. The diameter of a network is defined as the maximum shortest path between any pair of its nodes. It relates to the characteristic path length, which is the average number of links in the shortest path between two nodes. The smaller the diameter, the easier is the communication in the network.

2.1.2. Classical random networks. In these networks, the nodes are connected at random (Figure 1, right). In this case, the degree distribution is a Poisson distribution (the degree distribution, p_k, gives the probability that a node in the network is connected to k other nodes). The problem with these networks is that they have very small clustering coefficient and, thus, are not very stable. Removal of a number of nodes at random may fracture the network to noncommunicating parts. On the other hand, they are characterized by a small diameter. Far away nodes can be connected as easily as nearby nodes. In this case, information may be transported all over the network much more efficiently than in ordered networks. Thus, random networks exhibit efficient information transfer, but they are not stable.

2.1.3. Small-world networks. In nature, we should not expect to find either very regular or completely random networks. Rather, we should find networks that are efficient in processing information and at the same time are stable. Work in this direction led to a new type of network, which was proposed 12 years ago by the American mathematicians Duncan Watts and Steven Strogatz and is called *small-world* network [*Watts and Strogatz*, 1998]. A "small-world" network is a superposition of regular and classical random graphs. Such networks exhibit a high degree of local clustering, but a small number of long-range connections make

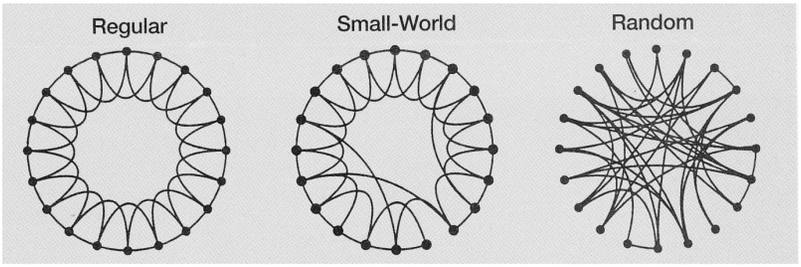

Figure 1. Illustration of a regular, a small-world, and a random network [after *Watts and Strogatz*, 1998]. Reprinted by permission from Macmillan Publishers Ltd: *Nature*, copyright 1998.

them as efficient in transferring information as random networks. Those long-range connections do not have to be designed. A few long-range connections added at random will do the trick (Figure 1, middle). The degree distribution of small-world networks is also a Poisson distribution.

2.1.4. Networks with a given degree distribution. The "small-world" architecture can explain phenomena such as the 6° of separation (most people are friends with their immediate neighbors, but we all have one or two friends a long way away), but it really is not a model found often in the real world. In the real world, the architecture of a network is neither random nor small-world, but it comes in a variety of distributions such as truncated power law distributions, Gaussian distributions, power law distributions, and distributions consisting of two power laws separated by a cutoff value (for a review, see *Strogatz* [2001]). The most interesting and common of such networks are the so-called *scale-free* networks. Consider a map showing an airline's routes. This map has a few hubs connecting with many other points (supernodes) and many points connected to only a few other points, a property associated with power law distributions. Such a map is highly clustered, yet it allows motion from a point to another far away point with just a few connections. As such, this network has the *property* of small-world networks, but this property is not achieved by local clustering and a few random connections. It is achieved by having a few elements with large number of links and many elements having very few links. Thus, even though they share the same property, the architecture of scale-free networks is different than that of "small-world" networks. Such inhomogeneous networks have been found to pervade biological, social, ecological, and economic systems, the Internet, and other systems [*Albert et al.*, 1999; *Liljeros et al.*, 2001; *Jeong et al.*, 2001; *Pastor-Satorras and Vespignani*, 2001; *Bouchaud and Mezard*, 2000; *Barabasi and Bonabeau*, 2003]. These networks are referred to as scale-free because they show a power law distribution of the number of links per node. Lately, it was also shown that, in addition to the power law degree distribution, many real scale-free networks consist of self-repeating patterns on all length scales [*Song et al.*, 2005]. These properties are very important because they imply some kind of self-organization within the network. Scale-free networks are not only efficient in transferring information, but due to the high degree of local clustering, they are also very stable [*Barabasi and Bonabeau*, 2003]. Because there are only a few super nodes, chances are that accidental removal of some nodes will not include the super nodes. In this case, the network would not become disconnected. This is not the case with weakly connected regular or random networks (and to a lesser degree with small-world networks), where accidental removal of the same percentage of nodes makes them more prone to failure [*Barabasi and Bonabeau*, 2003].

The topology of the network can reveal important and novel features of the system it represents [*Albert and Barabasi*, 2002; *Strogatz*, 2001; *Costa et al.*, 2007]. One such feature is communities [*Newman and Girvan*, 2004]. Communities represent groups of densely connected nodes with only a few connections between groups. It has been conjectured that each community represents a subsystem, which operates relatively independent of the other communities [*Arenas et al.*, 2006]. Thus, identification of these communities can offer useful insights about dynamics. In addition, communities can be associated to network functions such as in metabolic networks where certain groups of genes have been identified that perform specific functions [*Holme et al.*, 2003; *Guimera and Amaral*, 2005]. Recently, concepts from network theory have been applied to climate data organized as networks with impressive results [*Tsonis et al.*, 2006, 2007, 2008; *Tsonis and Swanson*, 2008; *Yamasaki et al.*, 2008; *Gozolchiani et al.*, 2008; *Swanson and Tsonis*, 2009; *Elsner et al.*, 2009; *Tsonis et al.*, 2010].

Figure 2 is an example of a climate network showing the area weighted connectivity (number of edges) at each geographic location for the 500 hPa height field [*Tsonis et al.*, 2006]. More accurately, it shows the fraction of the total global area that a point is connected to. This is a more appropriate way to show the architecture of the network because the network is a continuous network defined on a sphere. These data are derived from the global National Centers for Environmental Prediction/National Center for Atmospheric Research (NCEP/NCAR) atmospheric reanalysis data set [*Kistler et al.*, 2001]. The data are arranged on a grid with a resolution of 10° latitude × 10° longitude. This results in 36 points in the east-west direction and 19 points in the north-south direction for a total of $n = 684$ points. These 684 points are assumed to be the nodes of the network. For each grid point, monthly values from 1950 to 2005 are available. From the monthly values, anomaly values (actual value minus the climatological average for each month) are then produced. Even though the leading order effect of the annual cycle is removed by producing anomaly values, some of it is still present as the amplitude of the anomalies is greater in the winter than in the summer. For this reason, in order to avoid spurious high values of correlations, only the values for December–February in each year were considered. Thus, for each grid point, we have a time series of 168 anomaly values. In order to define the links between the nodes for either network, the correlation coefficient at lag zero (r) between the time series of all possible pairs of nodes [$n(n-1)/2 = 232,903$ pairs] is estimated. Note that since the

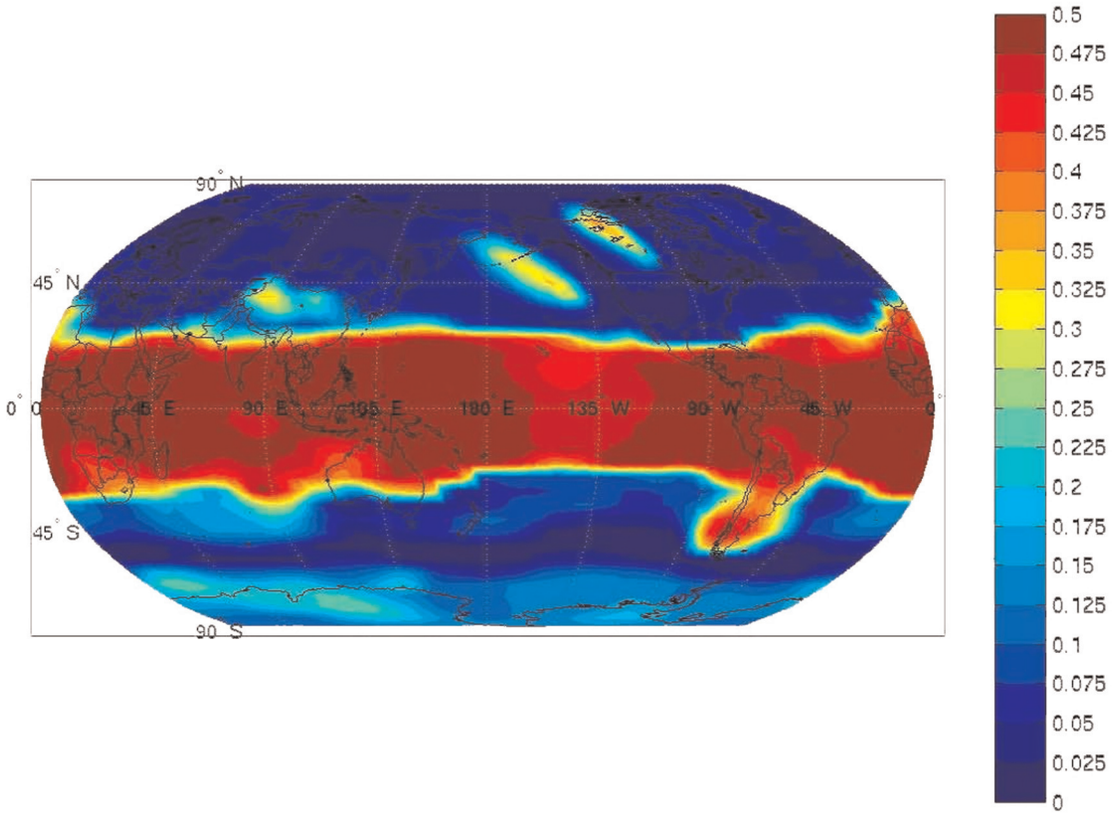

Figure 2. Total number of links (connections) at each geographic location. More accurately, it shows the fraction of the total global area that a point is connected to. This is a more appropriate way to show the architecture of the network because the network is a continuous network defined on a sphere. The uniformity observed in the tropics indicates that each node possesses the same number of connections. This is not the case in the extratropics where certain nodes possess more links than the rest.

values are monthly anomalies, there is very little autocorrelation in the time series.

A pair is considered as connected if the absolute value of their cross-correlation $|r| \geq 0.5$. This criterion is based on parametric and nonparametric significance tests. According to the t test with $N = 168$, a value of $r = 0.5$ is statistically significant above the 99% level. In addition, randomization experiments where the values of the time series of one node in a pair are scrambled and then are correlated to the unscrambled values of the time series of the other node indicate that a value of $r = 0.5$ will not arise by chance. The choice of $r = 0.5$, while it guarantees statistical significance, is somewhat arbitrary. We find that while other values might affect the connectivity structure of the network, the effect of different correlation thresholds (between 0.4 and 0.6) does not affect the conclusions. Obviously, as $|r| \to 1$, we end up with a random network, and as $r \to 0$, we remain with just one fully connected community. The use of the correlation coefficient to define links in networks is not new. Correlation coefficients have been used to successfully derive the topology of gene expression networks [*Farkas et al.*, 2003] and to study financial markets [*Mantegna*, 1999].

Returning to Figure 2, we observe two very interesting features. In the tropics, it appears that all nodes posses more or less the same (and high) number of connections, which is a characteristic of fully connected networks. In the extratropics, it appears that certain nodes posses more connections than the rest, which is a characteristic of scale-free networks. In the Northern Hemisphere, we clearly see the presence of regions where such supernodes exist in China, North America, and the northeast Pacific Ocean. Similarly, several supernodes are visible in the Southern Hemisphere. These differences between tropics and extratropics have been delineated in the corresponding degree distributions, which suggest that indeed the extratropical network is a scale-free

network characterized by a power law degree distribution [*Tsonis et al.*, 2006]. As is the case with all scale-free networks, the extratropical network is also a small-world network [*Tsonis et al.*, 2006].

An interesting observation in Figure 2 is that supernodes may be associated with major teleconnection patterns. For example, the supernodes in North America and northeast Pacific Ocean are located where the well-known Pacific North America (PNA) pattern [*Wallace and Gutzler*, 1981] is found. In the Southern Hemisphere, we also see supernodes over the southern tip of South America, Antarctica, and South Indian Ocean that are consistent with some of the features of the Pacific South America pattern [*Mo and Higgins*, 1998]. Interestingly, no such super nodes are evident where the other major pattern, the North Atlantic Oscillation (NAO) [*Thompson and Wallace*, 1998; *Pozo-Vazquez et al.*, 2001; *Huang et al.*, 1998] is found. This, however, does not indicate that NAO is an insignificant feature of the climate system. Since NAO is not strongly connected to the tropics, the high connectivity of the tropics with other regions is masking NAO out [*Tsonis et al.*, 2008].

Once the edges in a network have been defined, one can proceed with identifying the communities. Several methods of identifying communities were used. The first is based on the notion of node betweenness [*Girvan and Newman*, 2002]. For any node *i*, node betweenness is defined as the number of shortest paths between pairs of other nodes that run through *i*. The algorithm extends this definition to the case of edges, defining the "edge betweenness" of an edge as the number of shortest paths between pairs of nodes that run along this edge. If a network contains communities or groups that are only loosely connected by a few intergroup edges (think of bridges connecting different sections of New York City, for example), then all shortest paths between two nodes belonging to different communities must go along one of these few edges. Thus, the edges connecting communities will have high edge betweenness. By removing these edges, the groups are separated from one another thereby revealing the underlying community structure of the network.

Figure 3 illustrates the basics behind this algorithm. The setup is adapted from the work of *Newman and Girwan* [2004]. We start with a "source" node *s*, which is connected to six other nodes according to the simple network shown in Figure 3. This node is assigned a distance $d_s = 0$ and a weight $w_s = 1$. Then, each node *i* adjacent to *s* (i.e., nodes 1 and 3) is given a distance $d_i = d_s + 1$ and a weight $w_i = w_s$ (1,1 and 1,1, respectively). Then, each node *j* adjacent to nodes *i* is given a distance $d_j = d_i + 1$ and weight $w_j = w_i$ and so on. This procedure results in the pairs of values shown for each node. Once distances and weights have being assigned, one finds those nodes such that no shortest paths between any other node and *s* pass through them. Such nodes are nodes 2, 4, and 6. We call these nodes "leaves" and denote them as *l*. For each node *i* neighboring *l*, we assign a score to their edge of w_i/w_l. Accordingly, the score of the edges connecting pairs 1 and 2, 3 and 4, and 5 and 6 is equal to 1. Then, we start from the edge that is farther from *s* (that will be the edge connecting nodes 3 and 5) and assign a score that is 1 plus the sum of the scores on the neighboring edges immediately below it, multiplied by w_i/w_j where node *j* is farther from *s* than node *i*. We then move upward repeating the process until node *s* is reached. This procedure will identify the edge connecting nodes *s* and 3 as having the highest edge betweenness. By removing it, we remain with two communities, one consisting of nodes *s*, 1, and 2 and another consisting of nodes 3, 4, 5, and 6. We can then continue splitting the network by removing the edge with the second highest betweenness and so on. In applications with real data, however, this approach may not work well. The reason is that it may be that there is more than one edge connecting communities. In this case, there is no guarantee that all those edges will have high betweenness. We can only be sure that at least one will have high betweenness. For this reason, the algorithm repeats the whole process for all nodes in the network (i.e., considering as the source node each node in the network at a time) and sums all the scores. This gives the total betweenness for all edges in the network. We then have to repeat this calculation for each edge removed from the network. The network is then divided into two communities by removing the edge whose removal resulted in the lowest sum, and so on.

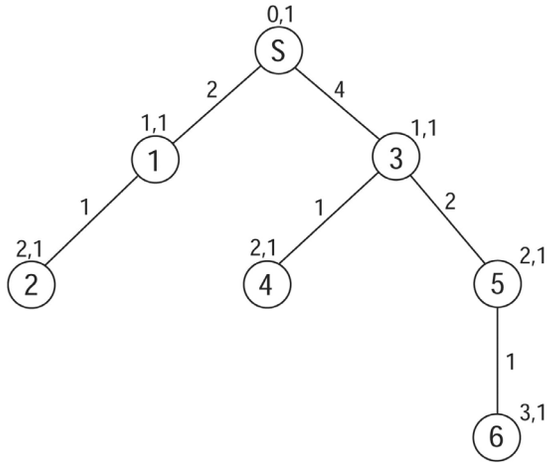

Figure 3. An illustration of the calculation of the shortest-path betweenness. See text for details.

In order to quantify the strength of a community structure, we use a measure called the *modularity*. For a

particular division into n communities, we define a $n \times n$ symmetric matrix **e** whose element e_{ij} is the fraction of all connections in the network that link nodes in community i to community j. The modularity [*Newman and Girvan*, 2004; *Girvan and Newman*, 2002; *Newman*, 2006] is defined as

$$Q = Tr\mathbf{e} - ||\mathbf{e}^2||,$$

where Tr is the trace of matrix **e** (the sum of the elements along the main diagonal), and $||x||$ indicates the sum of the elements of matrix $\boldsymbol{x}$. The modularity measures the fraction of the edges in the network that connect nodes of the same type (within-community nodes) minus the expected value of the same quantity in a network with the same community divisions but random connections between the nodes. Modularity ranges from zero (for random networks) to one (for very strong community structure). The optimum community division is found by estimating at how many communities (at what n) Q is maximum.

Figure 4 (left) shows the division into communities of three observed climate fields (the 500 hPa height, the global sea level pressure, and the global surface temperature fields [*Tsonis et al.*, 2010]. All fields are derived from the NCEP/NCAR atmospheric reanalysis data set [*Kistler et al.*, 2001]. Figure 4 (top) shows the community structure of the 500 hPa height network (shown in Figure 2), Figure 4 (middle) shows that of the sea level pressure network, and Figure 4 (bottom) shows that of the surface temperature network. The total number of communities is 47, 15, and 58, respectively. Many of these communities, however, consist of very few points in the boundaries between a small number of dominant communities (think of a country whose population is dominated by two races but also includes small groups of other races). As is evident in Figure 4, the effective number of communities is, arguably, four in all three networks (delineated as purple, blue, green, and yellow-red areas). The modularity of the networks is 0.49, 0.56, and 0.59, respectively, indicating networks that lie between completely random and strongly communal.

Importantly, this purely mathematical approach results in divisions that have connections with actual physics and dynamics. For example, in Figure 4 (top left) (500 hPa height network), we see that three of the effective four communities correspond to a latitudinal division 90°S–30°S, 30°S–30°N, and 30°N–90°N. This three-zone separation is not a trivial separation into Northern Hemisphere winter, Southern Hemisphere summer, and the rest of the world because when we repeat the analysis with yearly averages rather than seasonal values, we also see evidence of this three-zone separation. This separation is consistent with the transition from a barotropic atmosphere (where pressure depends on density only; appropriate for the tropics-subtropics) to a baroclinic atmosphere (where pressure depends on both density and temperature; appropriate for higher latitudes). Another possibility is that it reflects the well-known three-zone distribution of variance of the surface pressure field. Within the third community (green area) another community (yellow-red) is embedded. This community is consistent with the presence of major atmospheric teleconnection patterns such as the PNA pattern and the NAO [*Wallace and Gutzler*, 1981; *Barnston and Livezey*, 1987]. We note here that NAO (which has been lately suggested of being a three-pole pattern rather than a dipole) [*Tsonis et al.*, 2008] and Arctic Oscillation (AO) [*Thompson and Wallace*, 1998] are often interpreted as manifestations of the same dynamical mode, even though in some cases more physical meaning is given to NAO [*Ambaum et al.*, 2001]. In any case, here we do not make a distinction between NAO and AO.

In the sea level pressure network, we see again the latitudinal division into three communities. Here the purple area extends into the eastern Pacific as far as 30°N. This feature is consistent with the interhemispheric propagation of Rossby waves via the well-documented eastern Pacific corridor [*Webster and Holton*, 1982; *Tsonis and Elsner*, 1996]. The fourth community (yellow-red) embedded within the third community (green) is found over areas in the Northern Hemisphere where cyclogenesis is more frequently found. Note that PNA relates to anomalies in the forcing of extratropical quasistationary waves, the NAO arises from wave-mean flow interaction, and El Niño–Southern Oscillation (ENSO) is known to affect extratropical cyclone variability [*Eichler and Higgins*, 2006; *Wang and Fu*, 2000; *Held et al.*, 2002; *Favre and Gershunov*, 2006, 2009].

Figure 4. (opposite) Community structure in three climate networks. The networks are constructed from (top) the 500 hPa height field, (middle) the surface pressure field, and (bottom) the surface temperature field. Networks constructed (left) from observations and (right) from model simulations. The numbers below the shading key indicate the total number of communities. Because the total number of communities is not necessarily the same in each network, the color scheme used to show the spatial delineation of the communities is not the same in each plot. This means that the same community may be represented by a different color in the observations and in the model. The reverse may also be possible: the same color may not represent the same community. What we should compare in Figure 4 is the spatial distribution and structure of communities in observations and model (see text for more details).

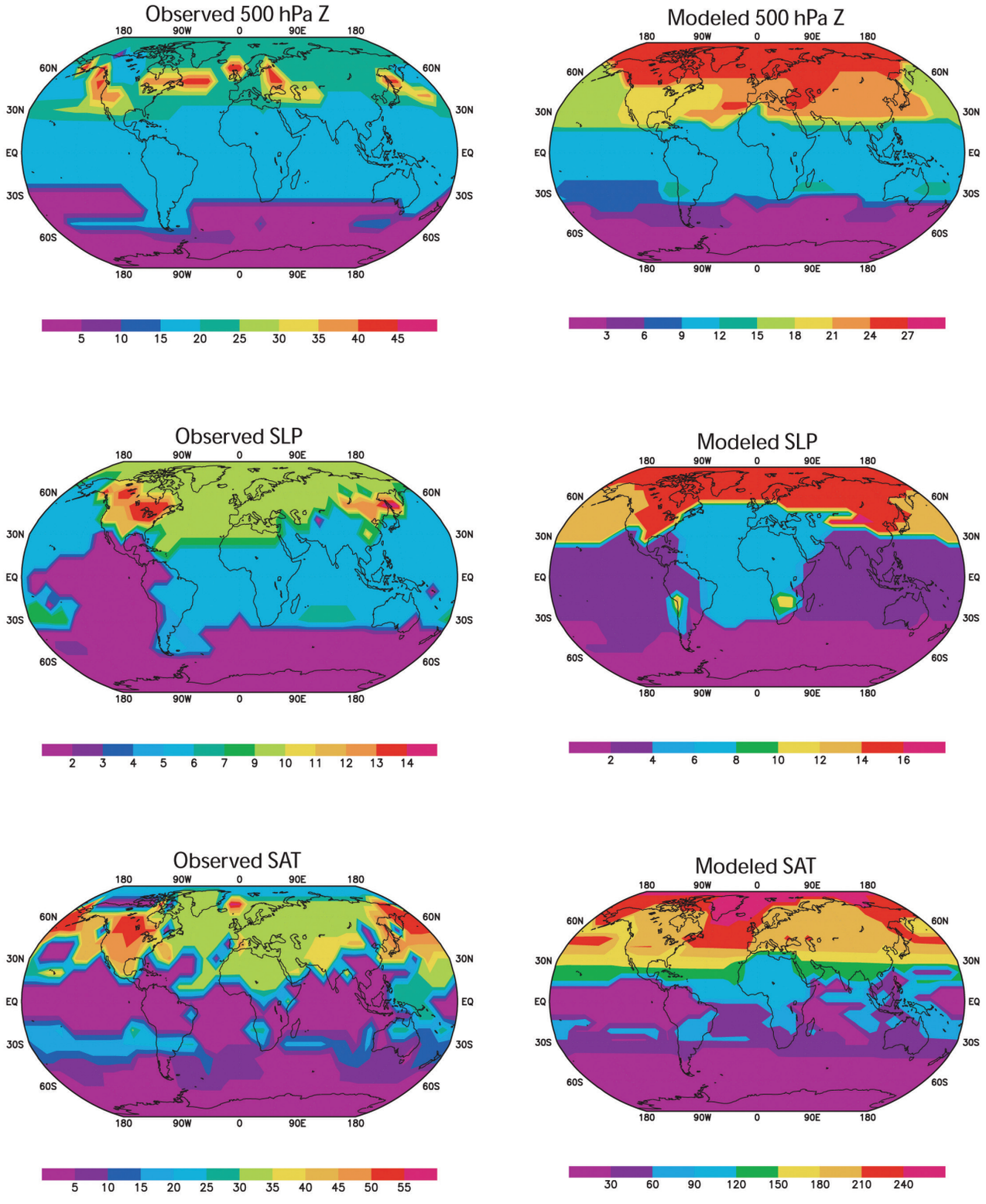
Observed 500 hPa Z
180 90W 0 90E 180
60N
30N
EQ
30S
60S
5 10 15 20 25 30 35 40 45
Modeled 500 hPa Z
3 6 9 12 15 18 21 24 27
Observed SLP
2 3 4 5 6 7 9 10 11 12 13 14
Modeled SLP
2 4 6 8 10 12 14 16
Observed SAT
5 10 15 20 25 30 35 40 45 50 55
Modeled SAT
30 60 90 120 150 180 210 240

Figure 4

In the temperature network, we see a major subdivision into two communities, one covering the Southern Hemisphere (purple) and the other the Northern Hemisphere (green). This appears to be a result of the fact that the Southern Hemisphere is covered mostly by water (which moderates surface temperatures), whereas the Northern Hemisphere is mostly land (where temperature variability is greater). In the Northern Hemisphere, we observe that embedded in the green community, there is a separate community (yellow-red) over North America and northeast Asia where cold winter air outbreaks normally occur. This could be an influence of the Pacific Decadal Oscillation (PDO), which is known to affect the North American temperature anomaly structure [*Mantua et al.*, 1997]. The green community, which includes the North Atlantic and Europe, may reflect the moderation of temperature fluctuations in the North Atlantic and Europe due to the Gulf Stream as a different community. In the Southern Hemisphere, embedded within the purple community, we see a separate community (blue) along the 30°S latitude. This community probably arises from the corresponding Southern Hemisphere storm tracks, which modify temperature fluctuations. Alternatively, it may be due to the presence of the subtropical belt. We note here that the location of some of the communities and their attributed teleconnection patterns may not be exactly the location of these patterns as delineated by empirical orthogonal function (EOF) analysis because they are different methods.

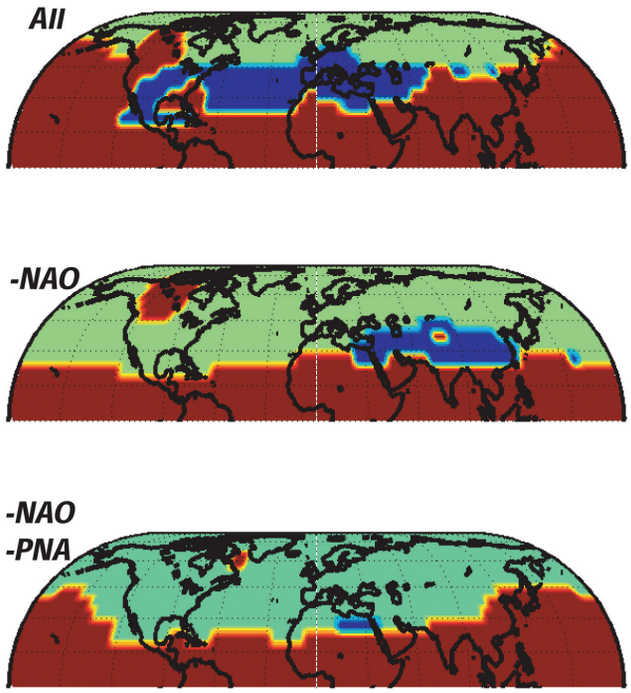

Figure 5. Community structure in the network for the observed 500 hPa height field in (top) the Northern Hemisphere as well as in the networks of synthetic 500 hPa height fields (middle) without the North Atlantic Oscillation (NAO) and (bottom) without the NAO and Pacific North America (PNA) (see text for details).

2.2. Sensitivity Analysis

The above analysis was repeated using detrended data as well as resampled data to obtain grids of equal area. The results were very similar to those in Figure 4. The division into communities for all three networks appears consistent with known dynamics and highlights the aspects of those dynamics that dominate interannual to decadal climate variability. In order to further strengthen the connection between communities and teleconnection patterns, the following experiment was performed: The observed 500 hPa field height in the Northern Hemisphere was considered, and as before, the corresponding network and its community structure were produced. This is the "null model," and its community structure is shown in Figure 5 (top) where three major communities (brown, green, and blue) are observed. Then, following the technique reported by *Tsonis et al.* [2008] and considering that EOF2 of the 500 hPa field is associated with NAO, a 500 hPa height field without the NAO was produced (by projecting the data to all but EOF2), the corresponding network was constructed, and its community structure was found (Figure 5, middle). Similarly, by considering that EOF1 of the 500 hPa filed is associated with the PNA, the PNA is removed as well (by projecting the data to all but EOF1 and EOF2) thereby producing a field without the PNA and without NAO. Then, the network is constructed, its community structure is found (Figure 5, bottom). It is observed that when NAO is removed, the blue community centered in the middle North Atlantic (where NAO occurs) has largely disappeared. A community identified by the blue color is still present but has shifted eastward and away from the area where NAO occurs. The brown community includes the tropics and a spot in North America located where the PNA pattern is found. This spot remains over the same area when the NAO is removed. That this spot is associated with the community, which includes the tropics, is consistent with the fact that the PNA is a linear response to tropical forcing. When the PNA is removed as well, the brown spot disappears. In Figure 5 (bottom), there is no sign of any kind that will be consistent with the PNA or NAO. This indicates that an "alternative model" that does not contain the kind of structure in which we are interested gives results outside the range of behavior produced by the "null model." Thus, attributing communities to teleconnection patterns is justified.

A number of additional network community sensitivity experiments were carried out. These experiments examined the network structure for spatiotemporal variability that is white with respect to time and spatially correlated with a decorrelation length of 3000 km on the sphere. A typical example of the character of the communities resulting from analyzing this type of noise is shown in Figure 6. In general, the following can be observed: (1) The number of communities is roughly the area of the sphere divided by the area of a circle of radius equal to the decorrelation length, i.e., for 3000 km, there are consistently 17–20 communities. (2) The community structure is nonrobust, as different realizations of the noise result in the same qualitative structure of communities (i.e., their number), but their position on the sphere is shifted. Even adding or subtracting 1 "year" from the synthetic data causes a leading order rearrangement in the position of the communities. Neither of these properties is consistent with what we observe for communities in the sea air temperature, sea level pressure, or 500 hPa height fields. In those observed fields, the number of communities is much smaller (about 5), and the structure of the communities is robust to adding or subtracting years from the analysis. Hence, it appears as if the observed community structure is not consistent with the structure arising from spatially correlated Gaussian white noise, and specifically, a null hypothesis that the observed structure can be reproduced using spatially correlated Gaussian white noise can safely be rejected.

2.3. Model Results

Returning to Figure 4, the right plots show the division into communities of networks constructed from model simulation of these three fields. The model used is the Geophysical Fluid Dynamics Laboratory (GFDL) CM2.1 coupled ocean/atmosphere model [*Delworth et al.*, 2006; *Gnanadesikan et al.*, 2006; *Wittenberg et al.*, 2006; *Stouffer et al.*, 2006]. The 1860 preindustrial conditions control run in the years 1950–2005 was used here. The resolution of these fields is also 10° × 10°. For the simulated fields, the number of communities is 27, 16, and 249, respectively. However, as with the observations, many of these communities include very few points in the boundaries of what appears to be about five dominant communities. The modularities of the networks are 0.55, 0.49, and 0.80, respectively, indicating again large differences from random networks. Note that because the number of communities is not necessarily the same in the model and in the observations, the color scheme used to show the spatial delineation of the communities is not the

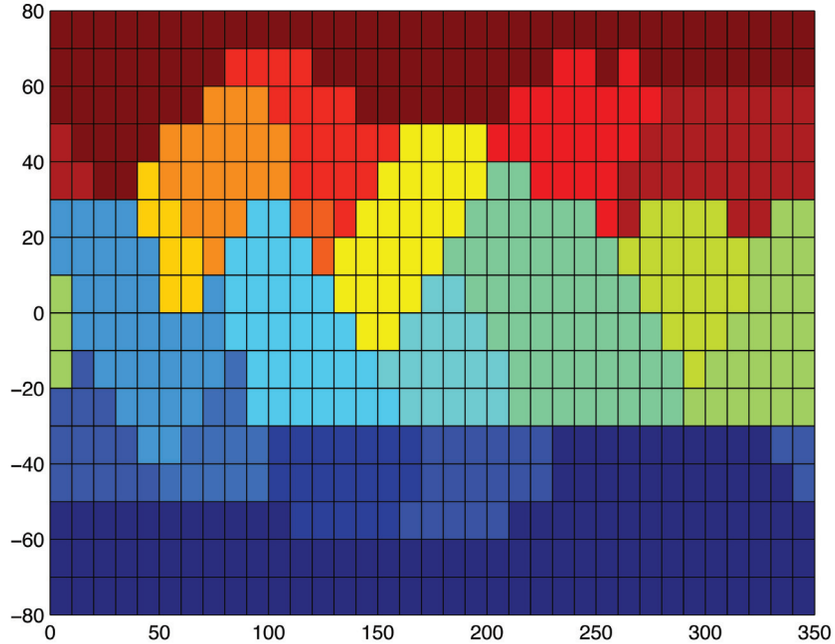

Figure 6. Community structure for a spatiotemporal variability that is white with respect to time and spatially correlated with a decorrelation length of 3000 km on the sphere. This structure is not consistent with the community structures shown in Figure 4. Thus, a null hypothesis that the observed structure in Figure 4 can be reproduced using spatially correlated Gaussian white noise can safely be rejected.

same in both observations and model simulations. This means that the same community may be represented by different colors in the observations and in the model. The reverse may also be possible: the same color may not represent the same community. What is relevant in comparing model simulations with observations in Figure 4 is the spatial distribution and structure of the most highly populated communities regardless of their assigned color.

The observed general subdivision into the three latitudinal zones in the 500 hPa height and sea level pressure networks, as well as the North Hemisphere-South Hemisphere division in the surface temperature network is well captured by the model. However, the detailed structure of the communities, especially in the Northern Hemisphere, is not well captured by the model simulations. This indicates limitations in the models' ability to adequately describe certain dynamical aspects. For example, in the temperature network (Figure 4, bottom right), the model does not reproduce a common community for the North Atlantic and Europe. This is consistent with insufficient resolution of oceanic sea surface temperatures (SSTs) and air-sea fluxes in the model to accurately delineate the moderation over Europe due to the heat transport of the Gulf Stream. Similarly, in the 500 hPa height network (Figure 4, top right), the model has difficulty reproducing the community structure associated with teleconnection patterns, indicating model deficiencies at simulating interannual atmospheric variability. In the sea level pressure network (Figure 4, middle right), it misses the Rossby waves emanation from the Southern Hemisphere to the Northern Hemisphere, marking model deficiencies in simulating the upper atmospheric flow over the tropical Pacific, a well-known problem in climate simulation [*Hack et al.*, 1998]. In spite of these structural differences, both model and observations agree that the number of communities is rather small.

This conclusion was verified by repeating the analysis using two additional different algorithms to divide the networks into communities. The first of these two approaches is based on finding the eigenvalues and eigenvectors of the modularity matrix [*Newman*, 2006]. The modularity matrix of the complete network is a real symmetric matrix B with elements

$$b_{ij} = a_{ij} - \frac{k_i k_j}{2M},$$

where a_{ij} are the elements of the adjacency matrix (equal to one if i and j are connected and zero otherwise), k_i is the number of connections of node i, and M is the total number of connections in the network. The method to split the network begins by estimating the eigenvalues and eigenvectors of the modularity matrix of the complete network. If all the elements in the eigenvector are of the same sign, there is only one community. Otherwise, according to the sign of the elements of this vector, the network is divided into two parts (communities). Next, this process is repeated recursively for each community (using now the community modularity matrix), and so on. The other approach is based on a Bayesian approach to network modularity [*Hofman and Wiggins*, 2008]. The results from these two approaches (not shown) are not significantly different from those in Figure 4. All methods delineate similar community structure with four to five effective communities. Note that due to spatial correlations, community structures do not change significantly when we consider the fields at a higher spatial resolution.

The above analysis brings up the more general question as to whether or not EOF analysis (which is based on variance explained) is indeed the appropriate method to study climate signals or oscillations. If variance is more important than how the system works (i.e., underlying topology), then EOF analysis may be a better approach. Otherwise, approaches like the network approach may be more appropriate. If there is an advantage of using networks, it is that the delineation of the major components is done "holistically" (meaning not in a set of EOFs), and it does not depend on the methodology and the assumptions used in estimating EOFs. The differences between the two methodologies may also account for possible mismatches in space between teleconnection patterns derived using network and EOF analysis. In any case, this is an important area of research, and it should be further pursued.

It thus appears that the full complexity of the climate system is, over the time scales used here, suppressed into a small number of relevant communities (subsystems). These communities involve major teleconnection patterns and climate modes such as the PNA and NAO, communication between the Southern Hemisphere and Northern Hemisphere, storm track dynamics, and the barotropic and baroclinic property of lower and higher latitudes, respectively. Having established the existence of subsystems, we then ask the question: what is their role and can their interaction explain decadal climate variability?

3. INTERACTION BETWEEN SUBSYSTEMS

One of the most important events in recent climate history is the climate shift in the mid-1970s [*Graham*, 1994]. In the Northern Hemisphere 500 hPa atmospheric flow, the shift manifested itself as a collapse of a persistent wave-3 anomaly pattern and the emergence of a strong wave-2 pattern. The shift was accompanied by SST cooling in the central Pacific and warming off the coast of western North America [*Miller*

et al., 1994]. The shift brought sweeping long-range changes in the climate of Northern Hemisphere. Incidentally, after "the dust settled," a new long era of frequent El Niño events superimposed on a sharp global temperature increase begun. While several possible triggers for the shift have been suggested and investigated [*Graham*, 1994; *Miller et al.*, 1994; *Graham et al.*, 1994], the actual physical mechanism that led to this shift is not known. Understanding the dynamics of such phenomena is essential for our ability to make useful prediction of climate change. A major obstacle to this understanding is the extreme complexity of the climate system, which makes it difficult to disentangle causal connections leading to the observed climate behavior. Next, a novel approach is presented, which reveals an important new mechanism in climate dynamics and explains several aspects of the observed climate variability in the late twentieth century.

First, a network from four major climate indices was constructed. The indices represent the PDO, the NAO, the ENSO, and the North Pacific Index (NPI) [*Barnston and Livezey*, 1987; *Hurell*, 1995; *Mantua et al.*, 1997; *Trenberth and Hurrell*, 1994]. These indices represent regional but dominant modes of climate variability, with time scales ranging from months to decades. NAO and NPI are the leading modes of surface pressure variability in northern Atlantic and Pacific Oceans, respectively, the PDO is the leading mode of SST variability in the northern Pacific, and ENSO is a major signal in the tropics. Together, these four modes capture the essence of climate variability in the Northern Hemisphere. Each of these modes is assumed to represent a subsystem involving different mechanisms over different geographical regions. Indeed, some of their dynamics have been adequately explored and explained by simplified models, which represent subsets of the complete climate system and which are governed by their own dynamics [*Elsner and Tsonis*, 1993; *Schneider et al.*, 2002; *Marshall et al.*, 2001; *Suarez and Schopf*, 1998]. For example, ENSO has been modeled by a simplified delayed oscillator in which the slower adjustment timescales of the ocean supply the system with the memory essential to oscillation. Monthly mean values in the interval 1900–2000 are available for all indices (see http://climatedataguide.ucar.edu/guidance/north-pacific-index-npi-trenberth-and-hurrell-monthly-and-winter).

These four climate indices are assumed to form a network of interacting nodes [*Tsonis et al.*, 2007]. A commonly used measure to describe variations in the network's topology is the mean distance $d(t)$ [*Onnela et al.*, 2005]:

$$d(t) = \frac{2}{N(N-1)} \sum_{d_{ij}^t \in D^t} d_{ij}^t. \qquad (1)$$

Here t denotes the time in the middle of a sliding window of width Δt, $N = 4$; $i, j = 1, \ldots, N$, and $d_{ij}^t = \sqrt{2\left(1 - |\rho_{ij}^t|\right)}$, where ρ_{ij}^t is the cross-correlation coefficient between nodes i and j in the interval $[t - (\Delta t - 1)/2, t + (\Delta t - 1)/2]$, and D^t is the $N \times N$ distance matrix. The sum is taken over the upper triangular part (or the distinct elements of D^t). The above formula uses the absolute value of the correlation coefficient because the choice of sign of indices is arbitrary. The distance can be thought of as the average correlation between all possible pairs of nodes and is interpreted as a measure of the synchronization of the network's components. Synchronization between nonlinear (chaotic) oscillators occurs when their corresponding signals converge to a common, albeit irregular, signal. In this case, the signals are identical, and their cross-correlation is 1. Thus, a distance of zero corresponds to a complete synchronization, and a distance of $\sqrt{2}$ signifies a set of uncorrelated nodes.

Figure 7a shows the distance as a function of time for a window length of Δt = 11 years, with tick marks corresponding to the year in the middle of the window. The correlations (and thus distance values for each year) were computed based on the annual mean indices constructed by averaging the monthly indices over the period of November–March. The dashed line parallel to the time axis in Figure 7a represents the 95% significance level associated with the null hypothesis that the observed indices are sampled from a population of a 4-D autoregressive-1 (AR-1) process driven by a spatially (cross-index) correlated Gaussian noise; the parameters of the AR-1 model and the covariance matrix of the noise are derived from the full time series of the observed indices. This test assumes that the variations of the distance with time seen in Figure 7a are due to sampling associated with a finite-length (11 years) sliding window used to compute the local distance values. Retaining overall cross-correlations in constructing the surrogates makes this test very stringent. Nevertheless, we still find that at five times (1910s, 1920s, 1930s, 1950s, and 1970s), distance variations fall below the 95% significance level. We therefore conclude that these features are not likely to be due to sampling limitations, but they represent statistically significant synchronization events. Note that the window length used in Figure 7a is a compromise between being long enough to estimate correlations but not too long to "dilute" transitions. Nevertheless, the observed synchronizations are insensitive to the window size in a wide range of 7 years $\leq \Delta t \leq$ 15 years.

An important aspect in the theory of synchronization between coupled nonlinear oscillators is coupling strength. It is vital to note that synchronization and coupling are not interchangeable; for example, it is trivial to construct a pair of coupled simple harmonic oscillators whose displacements

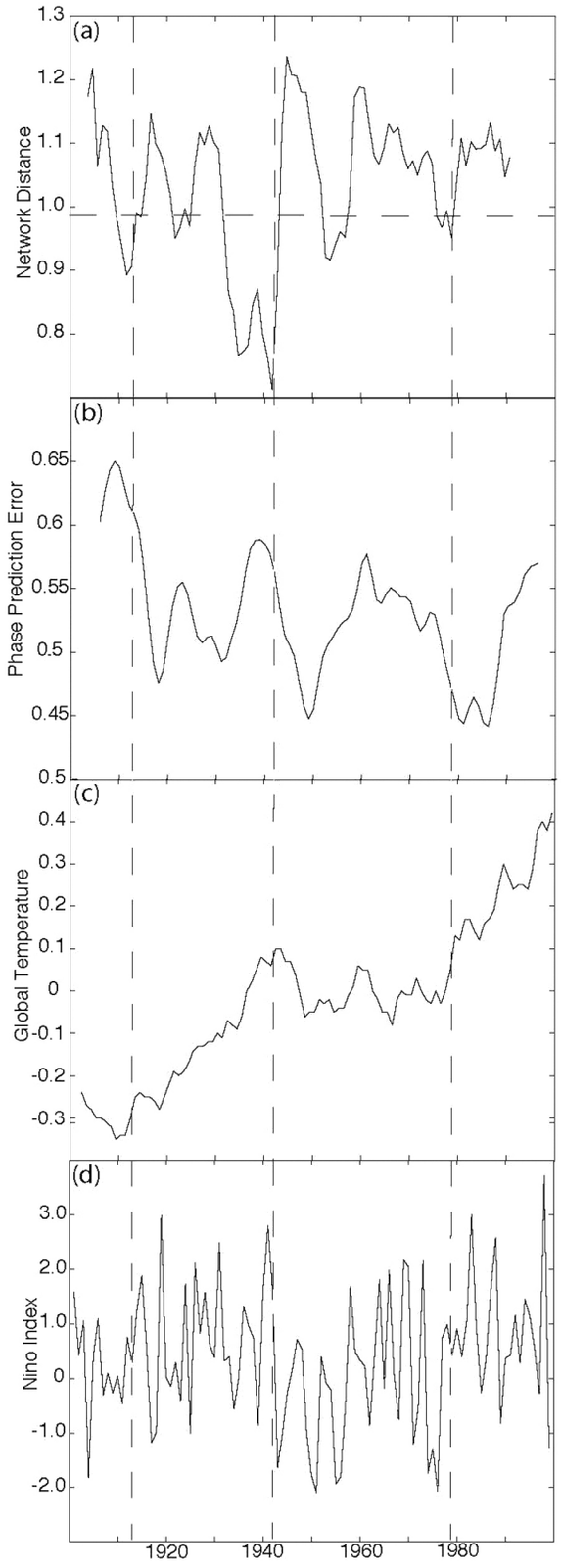

are in quadrature (and, hence, perfectly uncorrelated), but whose phases are strongly coupled [*Vanassche et al.*, 2003]. As such, coupling is best measured by how strongly the phases of different modes of variability are linked. The theory of synchronized chaos predicts that in many cases when such systems synchronize, an increase in coupling between the oscillators may destroy the synchronous state and alter the system's behavior [*Heagy et al.*, 1995; *Pecora et al.*, 1997]. In view of the results above, the question thus arises as to how the synchronization events in Figure 7a relate to coupling strength between the nodes. It should be noted that in this study, the focus is in the complete synchronization among the nodes, rather than weaker types of synchronization, such as phase synchronization [*Boccaletti et al.*, 2002; *Maraun and Kurths*, 2005] or clustered synchronization [*Zhou and Kurths*, 2006], which are also important in climate interactions.

For our purposes here, if future changes in the phase between pairs of climate modes can be readily predicted using only information about the current phase, those modes may be considered strongly coupled [*Smirnov and Bezruchko*, 2003]. Here in order to study coupling, symbolic dynamics are used. For any given time series point, we can define a symbolic phase by examining the relationship between that point and its nearest two neighbors in time. As shown in Figure 8, if the three points are sequentially increasing, we can assign to the middle point a phase of 0 while, if they are sequentially decreasing, a phase of π. Intermediate values then follow. Notice that this procedure is totally nonparametric, as it does not compare the actual values of the points aside from whether a point is larger or smaller than its neighbors. The advantage of this approach is that it is blind to ultralow-frequency variability, i.e., decadal scale and longer. Use of symbolic dynamics is appropriate in this case, as we are primarily interested in changes in the synchronicity and coupling of climate modes over decadal time scales. The symbolic phase ϕ_n^j is constructed separately for the four climate indices, where *j* denotes the index, and *n* denotes the

Figure 7. (opposite) (a) The distance (see definition in text) of a network consisting of four observed major climate modes as a function of time. This distance is an indication of synchronization between the modes with smaller distance implying stronger synchronization. The parallel dashed line represents the 95% significance level associated with a null hypothesis of spatially correlated red noise. (b) Coupling strength between the four modes as a function of time. (c) The global surface temperature record. (d) Global sea surface temperature El Niño–Southern Oscillation index. The vertical lines indicate the time when the network goes out of synchronization for those cases where synchronization is followed by a coupling strength increase.

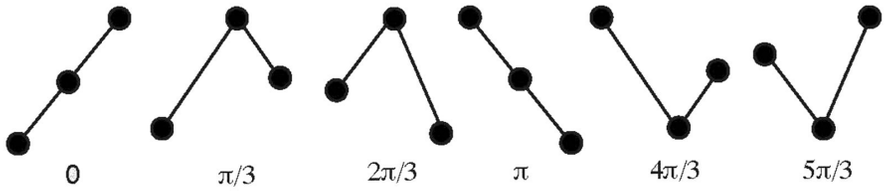

Figure 8. The six states for the symbolic phase construction. The points in each triplet correspond to three consecutive points in a time series, and their relative vertical positions to each other indicate their respective values.

year. The phases for a given year n are represented by the complex phase vector $\overrightarrow{Z_n}$ with elements $Z_n^j = \exp(i\phi_n^j)$. The predictability of this phase vector from year to year provides a measure of the coupling and is determined using the least squares estimator

$$\overrightarrow{Z}_{n+1}^{est} = \mathbf{M}\,\overrightarrow{Z_n}, \tag{2}$$

where $\mathbf{M} = [\mathbf{Z}_+\mathbf{Z}^{\mathrm{T}}]\,[\mathbf{Z}\mathbf{Z}^{\mathrm{T}}]^{-1}$ is the least squares predictor. Here $\mathbf{Z}$ and $\mathbf{Z}_+$ are the matrices whose columns are the vectors $\overrightarrow{Z_n}$ and $\overrightarrow{Z_{n+1}}$, respectively, constructed using allyears. A measure of the coupling then is simply $||\overrightarrow{Z}_{n+1}^{est} - \overrightarrow{Z_{n+1}}||^2$, where strong coupling is associated with small values of this quantity, i.e., good phase prediction. Note that only three values are used to define phases rather than four or five or any other number. The reason is that the possible number of permutations of m values is $m!$ Thus, if $m > 3$, there is at least 24 possible permutations, which will not result in large sample sizes to evaluate the predictability of the phase vector.

This quantity is plotted in Figure 7b. Figures 7c and 7d show the global surface temperature (http://data.giss.nasa.gov/gistemp/) and El Niño index in our period. Figure 7 tells a remarkable story. First, let us consider the event in the 1910s. The network synchronizes at about 1910. At that time, the coupling strength begins to increase. Eventually, the network comes out of the synchronous state sometime in late 1912, early 1913 (marked by the left vertical line). The destruction of the synchronous state coincides with the beginning of a sharp global temperature increase and a tendency for more frequent and strong El Niño events. The network enters a new synchronization state in the early 1920s, but this is not followed by an increase in coupling strength. In this case, no major shifts are observed in the behavior of global temperature and ENSO. Then, the system enters a new synchronization state in the early 1930s. Initially, this state was followed by a decrease in coupling strength, and again, no major shifts are observed. However, in the early 1940s, the still present synchronous state is subjected to an increase in coupling strength, which soon destroys it (at the time indicated by the middle vertical line). As the synchronous state is destroyed, a new shift in both temperature trend and ENSO variability is observed. The global temperature enters a cooling regime, and El Niño events become much less frequent and weaker. The network synchronizes again in the early 1950s. This state is followed by a decrease in coupling strength, and as was the case in 1920s, no major shifts occur. Finally, the network synchronizes again in the mid-1970s. This state is followed by an increase in coupling strength, and incredibly, as in the cases of 1910s and 1940s, synchronization is destroyed (at the time marked by the right vertical line), and then, climate shifts again. The global temperature enters a warming regime, and El Niño events become frequent and strong. The fact that around 1910, 1940, and in the late 1970s climate shifted to a completely new state indicates that synchronization followed by an increase in coupling between the modes leads to the destruction of the synchronous state and the emergence of a new state.

The above mechanism was also found in three climate simulations. The first two are from the GFDL CM2.1 coupled ocean/atmosphere model [*Delworth et al.*, 2006; *Gnanadesikan et al.*, 2006; *Wittenberg et al.*, 2006; *Stouffer et al.*, 2006]. The first simulation is an 1860 preindustrial condition, 500 year control run, and the second is the SRESA1B, which is a "business as usual" scenario with CO_2 levels stabilizing at 720 ppmv at the close of the twenty-first century [*Intergovernmental Panel on Climate Change*, 2001]. The third simulation is a control run from the ECHAM5 model [*Tsonis et al.*, 2007; *Wang et al.*, 2009]. From these model outputs, we constructed the same indices (in the periods of 100–200 years, twenty-first century, and years 240–340, respectively) and repeated the above procedure to study synchronization and coupling in the corresponding networks. In all, we found seven synchronization events in the model simulations. As with the five synchronization events in the observations in the twentieth century shown in Figure 7, here as well, without an exception in all cases when the major modes of variability in the Northern Hemisphere are synchronized, an increase in the coupling strength destroys the synchronous state and causes climate to shift to a new state. Importantly, the mechanism is found in both forced and unforced simulations indicating that the mechanism is a result of the natural

variability of the climate system. Lately, *Swanson and Tsonis* [2009] extended the analysis to the updated observations in the twenty-first century and discovered yet another consistent event signaling a new climate shift in the beginning of the twenty-first century.

The shifts described above are based on careful visual examination of the results. Once shifts have been visually identified, one can statistically test their significance. From the above results, it was observed [*Tsonis et al.*, 2007; *Wang et al.*, 2009] that most often a shift in global temperature can manifest itself as a trend change, but in a couple of cases, it shows as a jump. Changes in ENSO variability, on the other hand, can come in more ways. In this case, the possible regimes are five. A regime of more frequent El Niño events, a regime of more frequent La Niña events, a regime of alternating strong El Niño and La Niña events, a regime of no activity or alternating weak El Niño and La Niña events, and a regime where the spacing between El Niño and La Niña events is irregular. In all those regimes, the distribution of ENSO index is different, and as such, the Mann-Whitney rank sum test can be used to test for differences before and during a shift or between shifts. The same test can be used to test differences in global temperature tendency before and after a jump. In cases when a temperature tendency shift manifests itself as a trend change, the *t* test can be used. In all, 12 synchronization events and eight shifts occurred in observations and model simulations (not including the suspected shift in the twenty-first century observations). For all shifts (three in observations and five in the models), it was found that the change in ENSO variability is significant at the 90% or higher confidence level, whereas the change in temperature tendency is significant at the 95% or higher confidence level (see supplementary material of *Wang et al.* [2009]).

The above results refer to the collective behavior of the four major modes used in the network. As such, they do not offer insights on the specific details of the mechanism. For example, do small distance values (strong synchronization) result from all modes synchronizing or from a subset of them? When the network is synchronized, does the coupling increase require that all modes must become coupled with each other? To answer these questions, *Wang et al.* [2009] split the network of four modes into its six pair components and investigated the contribution of each pair in each synchronization event and in the overall coupling of the network. It was found that one mode is behind all climate shifts. This mode is the NAO. This North Atlantic mode is without exception the common ingredient in all shifts, and when it is not coupled with any of the Pacific modes, no shift ensues. In addition, in all cases where a shift occurs, NAO is necessarily coupled to North Pacific. In some cases, it may also be coupled to the tropical Pacific (ENSO) as well, but in none of the cases, NAO is only coupled to ENSO. Thus, results indicate that not only NAO is the instigator of climate shifts but also that the likely evolution of a shift has a path where the North Atlantic couples to the North Pacific, which, in turn, couples to the tropics. Solid dynamical arguments and past work offer a concrete picture of how the physics may play out. NAO with its huge mass rearrangement in North Atlantic affects the strength of the westerly flow across midlatitudes. At the same time through its "twin," the AO, it impacts sea level pressure patterns in the northern Pacific. This process is part of the so-called intrinsic midlatitude Northern Hemisphere variability [*Vimont et al.*, 2001, 2003]. Then, this intrinsic variability through the seasonal footprinting mechanism [*Vimont et al.*, 2001, 2003] couples with equatorial wind stress anomalies, thereby acting as a stochastic forcing of ENSO. This view is also consistent with a recent study showing that PDO modulates ENSO [*Gershunov and Barnett*, 1998; *Verdon and Franks*, 2006]. Another possibility of how NAO couples to the North Pacific may be through the five-lobe circumglobal waveguide pattern [*Branstator*, 2002]. It has been shown that this waveguide pattern projects onto NAO indices, and its features contribute to variability at locations throughout the Northern Hemisphere. Finally, the North Atlantic variations have been linked to the Northern Hemisphere mean surface temperature multidecadal variability through redistribution of heat within the northern Atlantic with the other oceans left free to adjust to these Atlantic variations [*Zhang et al.*, 2007]. Thus, NAO, being the major mode of variability in the northern Atlantic, impacts both ENSO variability and global temperature variability. Recently, a study has shown how ENSO with its effects on PNA can, through vertical propagation of Rossby waves, influence the lower stratosphere and how in turn the stratosphere can influence NAO through downward progression of Rossby wave [*Ineson and Scaife*, 2009]. These results, coupled with our results, suggest the following 3-D superloop: NAO → PDO → ENSO → PNA → stratosphere → NAO, which captures the essence of decadal variability in the Northern Hemisphere and possibly the globe.

It is interesting to compare Figure 2 and the top left plot of Figure 4. Apparently, there are similarities (the three-zone separation, for example), but the community algorithm identifies NAO clearly, whereas in Figure 2, as we mentioned earlier, NAO is masked. Owing to barotropic conditions in the tropical areas, communication via gravity waves is fast, and as result, the information flows very efficiently resulting in a fully connected network in the tropics. In the extratropics, supernodes are found in locations where major teleconnection patterns are found, which, in turn, define distinct communities in the network. It may be that in spatially extended systems with spatial correlations extending over a

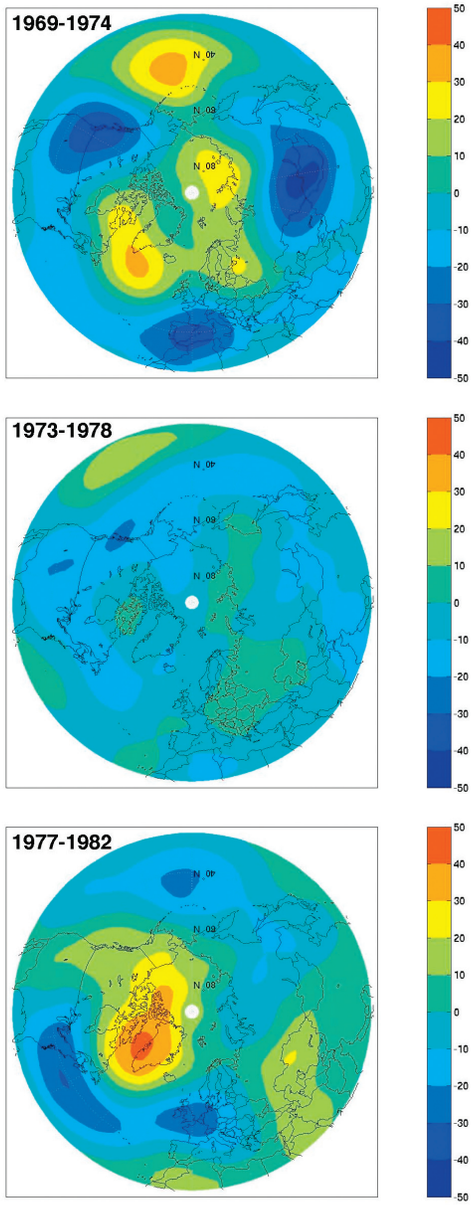

Figure 9. The 500 hPa anomaly field composites for the periods (top) 1969–1974, (middle) 1973–1978, and (bottom) 1977–1982. A wave-3 pattern is visible in the top plot with PNA and NAO in its negative phase being present. In the middle plot, both NAO and PNA have, for all practical purposes, disappeared. In the bottom plot, the field emerges as a wave-2 pattern with NAO in its positive phase. As we explain in the text, this transition (known as the climate shift of the 1970s) is consistent with our conjecture that removal of supernodes makes the (climate) network unstable and more prone to failure (breakdown of a regime and emergence of another regime).

characteristic scale, the connectivity pattern is related to community structure. In any case, since the presence of super nodes makes the network stable and efficient in transferring information, it was speculated and shown that, indeed, teleconnection patterns act as climate stabilizers. *Tsonis et al.* [2008] have shown that removal of teleconnection patterns from the climate system results in less stable networks, which make an existing climate regime unstable and more likely to shift to a new regime. Indeed, they showed that this process may be behind the climate shift of the 1970s and related to the dynamical mechanism for major climate shifts discussed above. Figure 9 shows 500 hPa anomaly composites for three 5 year periods in the 1970s and early 1980s. In the early 1970s (Figure 9, top), the 500 hPa anomaly field is dominated by the presence of a wave-3 pattern with both the PNA and NAO (in its negative phase) being very pronounced. In the mid-1970s (Figure 9, middle), this field is very weak, and both NAO and PNA have, for all practical purposes, disappeared. After that (Figure 9, bottom), the field becomes strong again, but a new wave-2 pattern with a very pronounced positive NAO has emerged. This shift is known as the climate shift of the 1970s. According to the *Tsonis et al.* [2007] mechanism for major climate shifts, climate modes may synchronize. Once in place, the synchronized state may become unstable and shift to a new state. The results of *Tsonis et al.* [2008] and those in Figure 9 suggest a connection between stability, synchronization, coupling of major climate modes, and climate shifts. This point is the subject of our continuing work in this area, and more results will be forthcoming in the future.

As a final note before concluding, it should be mentioned that lately, *Tsonis and Swanson* [2011] extended their approach to consider proxy data for climate modes going back several centuries. While noise in the proxy data, in some cases, masks the mechanism, it was found that significant coherence between both synchronization and coupling and global temperature exists. These results provide further support that the mechanism for climate shifts discussed here is a robust feature of the climate system.

4. CONCLUSIONS

The above synthesis describes some new approaches that have been applied lately to climate data. The findings presented here may settle the issue of dimensionality of climate variability over decadal scales, as they support the view that over these scales, climate collapses into distinct subsystems whose interplay dictates decadal variability. At the same time, these results provide clues as to what these subsystems might be. As such, while “weather” may be complicated, “climate” may be complex but not complicated. Moreover, it

appears that the interaction between these subsystems may be largely responsible for the observed decadal climate variability. A direct consequence of these results is that a dynamical reconstruction directly from a small number of climate modes/subsystems may be attempted to extract differential equations, which model the network of major modes. Such an approach may provide an alternative and direct window to study low-frequency variability in climate. Work in this area is in progress and will be reported in the future elsewhere.

Acknowledgment. This work was supported by NSF grant AGS-0902564.

REFERENCES

Albert, R., and A.-L. Barabasi (2002), Statistical mechanics of complex networks, *Rev. Mod. Phys.*, *74*, 47–101.

Albert, R., H. Jeong, and A.-L. Barabasi (1999), Diameter of the World Wide Web, *Nature*, *401*, 130–131.

Ambaum, M. H. P., B. J. Hoskins, and D. B. Stephenson (2001), Arctic Oscillation or North Atlantic Oscillation?, *J. Clim.*, *14*, 3495–3507.

Arenas, A., A. Diaz-Guilera, and C. J. Perez-Vicente (2006), Synchronization reveals topological scales in complex networks, *Phys. Rev. Lett.*, *96*, 114102, doi:10.1103/PhysRevLett.96.114102.

Barabasi, A.-L., and E. Bonabeau (2003), Scale-free networks, *Sci. Am.*, *288*, 60–69.

Barnston, A. G., and R. E. Livezey (1987), Classification, seasonality, and persistence of low-frequency atmospheric circulation patterns, *Mon. Weather Rev.*, *115*, 1083–1126.

Branstator, G. (2002), Circumglobal teleconnections, the jet stream waveguide, and the North Atlantic Oscillation, *J. Clim.*, *15*, 1893–1910.

Boccaletti, S., J. Kurths, G. Osipov, D. J. Valladares, and C. S. Zhou (2002), The synchronization of chaotic systems, *Phys. Rep.*, *366*, 1–101.

Bouchaud, J.-P., and M. Mezard (2000), Wealth condensation in a simple model of economy, *Physica A*, *282*, 536–540.

Costa, L. D. F., F. A. Rodrigues, G. Travieso, and P. R. Villas Boas (2007), Characterization of complex networks: A survey of measurements, *Adv. Phys.*, *56*, 167–242.

Delworth, T. L., et al. (2006), GFDL's CM2 global coupled climate models. Part I: Formulation and simulation characteristics, *J. Clim.*, *19*, 643–674.

Eichler, T., and R. W. Higgins (2006), Climatology and ENSO-related variability of North American extratropical cyclone activity, *J. Clim.*, *19*, 2076–2093.

Elsner, J. B., and A. A. Tsonis (1993), Nonlinear dynamics established in the ENSO, *Geophys. Res. Lett.*, *20*(3), 213–216.

Elsner, J. B., T. H. Jagger, and E. A. Fogarty (2009), Visibility network of United States hurricanes, *Geophys. Res. Lett.*, *36*, L16702, doi:10.1029/2009GL039129.

Farkas, I. J., H. Jeong, T. Vicsek, A.-L. Barabási, and Z. N. Oltvai (2003), The topology of the transcription regulatory network in the yeast *Saccharomyces cerevisiae*, *Physica A*, *318*, 601–612.

Favre, A., and A. Gershunov (2006), Extra-tropical cyclonic/anticyclonic activity in north-eastern Pacific and air temperature extremes in western North America, *Clim. Dyn.*, *26*, 617–629.

Favre, A., and A. Gershunov (2009), North Pacific cyclonic and anticyclonic transients in a global warming context: Possible consequences for western North American daily precipitation and temperature extremes, *Clim. Dyn.*, *32*, 969–987.

Gershunov, A., and T. P. Barnett (1998), Interdecadal modulation of ENSO teleconnections, *Bull. Am. Meteorol. Soc.*, *79*, 2715–2725.

Girvan, M., and M. E. J. Newman (2002), Community structure in social and biological networks, *Proc. Natl. Acad. Sci. U. S. A.*, *99*, 7821–7826.

Gnanadesikan, A., et al. (2006), GFDL's CM2 global coupled climate models. Part II: The baseline ocean simulation, *J. Clim.*, *19*, 675–697.

Gozolchiani, A., K. Yamasaki, O. Gazit, and S. Havlin (2008), Pattern of climate network blinking links follow El Niño events, *Europhys. Lett.*, *83*, 28005, doi:10.1209/0295-5075/83/28005.

Graham, N. E. (1994), Decadal scale variability in the tropical and North Pacific during the 1970s and 1980s: Observations and model results, *Clim. Dyn.*, *10*, 135–162.

Graham, N. E., T. P. Barnett, R. Wilde, M. Ponater, and S. Schubert (1994), On the roles of tropical and mid-latitude SSTs in forcing interannual to interdecadal variability in the winter Northern Hemisphere circulation, *J. Clim.*, *7*, 1500–1515.

Guimera, R., and L. A. N. Amaral (2005), Functional cartography of complex metabolic network, *Nature*, *433*, 895–900.

Hack, J. J., J. T. Kiehl, and J. W. Hurrell (1998), The hydrologic and thermodynamic characteristics of NCAR CCM3, *J. Clim.*, *11*, 1179–1206.

Heagy, J. F., L. M. Pecora, and T. L. Carroll (1995), Short wavelength bifurcations and size instabilities in coupled oscillator systems, *Phys. Rev. Lett.*, *74*, 4185–4188.

Held, I. M., M. Ting, and H. Wang (2002), Northern winter stationary waves: Theory and modeling, *J. Clim.*, *15*, 2125–2144.

Hofman, J. M., and C. H. Wiggins (2008), A Bayesian approach to network modularity, *Phys. Rev. Lett.*, *100*, 258701, doi:10.1103/PhysRevLett.100.258701.

Holme, P., M. Huss, and H. Jeong (2003), Subnetwork hierarchies of biochemical pathways, *Bioinformatics*, *19*, 532–543.

Huang, J., K. Higuchi, and A. Shabbar (1998), The relationship between the North Atlantic Oscillation and El Niño-Southern Oscillation, *Geophys. Res. Lett.*, *25*(14), 2707–2710.

Hurrell, J. W. (1995), Decadal trends in the North Atlantic oscillation regional temperature and precipitation, *Science*, *269*, 676–679.

Ineson, S., and A. A. Scaife (2009), The role of the stratosphere in the European climate response to El Niño, *Nature Geosci.*, *2*, 32–36.

Intergovernmental Panel on Climate Change (2001), *Climate Change 2001: The Scientific Basis: Contribution of Working Group I to the Third Assessment Report of the Intergovernmental*

Panel on Climate Change, edited by J. T. Houghton et al., 881 pp., Cambridge Univ. Press, New York.

Jeong, H., S. Mason, A.-L. Barabasi, and Z. N. Oltvai (2001), Lethability and centrality in protein networks, *Nature*, *411*, 41–42.

Kistler, R., et al. (2001), The NCEP/NCAR 50-year reanalysis: Monthly means, CD-ROM and documentation, *Bull. Am. Meteorol. Soc.*, *82*, 247–267.

Liljeros, F., C. Edling, L. N. Amaral, H. E. Stanley, and Y. Aberg (2001), The web of human sexual contacts, *Nature*, *411*, 907–908.

Lorenz, E. N. (1991), Dimension of weather and climate attractors, *Nature*, *353*, 241–244.

Mantegna, R. N. (1999), Hierarchical structure in financial markets, *Eur. Phys. J. B*, *11*, 193–197.

Mantua, N. J., S. R. Hare, Y. Zhang, J. M. Wallace, and R. C. Francis (1997), A Pacific interdecadal climate oscillation with impacts on salmon production, *Bull. Am. Meteorol. Soc.*, *78*, 1069–1079.

Maraun, D., and J. Kurths (2005), Epochs of phase coherence between El Niño/Southern Oscillation and Indian monsoon, *Geophys. Res. Lett.*, *32*, L15709, doi:10.1029/2005GL023225.

Marshall, J., et al. (2001), North Atlantic climate variability: Phenomena, impacts and mechanisms, *Int. J. Climatol.*, *21*, 1863–1898.

Miller, A. J., D. R. Cayan, T. P. Barnett, N. E. Craham, and J. M. Oberhuber (1994), The 1976–77 climate shift of the Pacific Ocean, *Oceanography*, *7*, 21–26.

Mo, K. C., and R. W. Higgins (1998), The Pacific-South America modes and tropical convection during the Southern Hemisphere winter, *Mon. Weather Rev.*, *126*, 1581–1596.

Nerenberg, M. A. H., and C. Essex (1990), Correlation dimension and systematic geometric effects, *Phys. Rev. A*, *42*, 7065–7074.

Newman, M. E. J. (2006), Modularity and community structure in networks, *Proc. Natl. Acad. Sci. U. S. A.*, *103*, 8577–8582.

Newman, M. E. J., and M. Girvan (2004), Finding and evaluating community structure in networks, *Phys. Rev. E*, *69*, 026113, doi:10.1103/PhysRevE.69.026113.

Nicolis, C., and G. Nicolis (1984), Is there a climatic attractor?, *Nature*, *311*, 529–532.

Onnela, J.-P., J. Saramaki, J. Kertesz, and K. Kaski (2005), Intensity and coherence of motifs in weighted complex networks, *Phys. Rev. E*, *71*, 065103, doi:10.1103/PhysRevE.71.065103.

Pastor-Satorras, R., and A. Vespignani (2001), Epidemic spreading in scale-free networks, *Phys. Rev. Lett.*, *86*, 3200–3203.

Pecora, L. M., T. L. Carroll, G. A. Johnson, and D. J. Mar (1997), Fundamentals of synchronization in chaotic systems, concepts, and applications, *Chaos*, *7*, 520–543.

Pozo-Vazquez, D., M. J. Esteban-Parra, F. S. Rodrigo, and Y. Castro-Diez (2001), The association between ENSO and winter atmospheric circulation and temperature in the North Atlantic region, *J. Clim.*, *14*, 3408–3420.

Schneider, N., A. J. Miller, and D. W. Pierce (2002), Anatomy of North Pacific decadal variability, *J. Clim.*, *15*, 586–605.

Smirnov, D. A., and B. P. Bezruchko (2003), Estimation of interaction strength and direction from short and noisy time series, *Phys. Rev.*, *68*, 046209, doi:10.1103/PhysRevE.68.046209.

Smith, L. A. (1988), Intrinsic limits on dimension calculations, *Phys. Lett. A*, *133*, 283–288.

Song, C., S. Havlin, and H. A. Makse (2005), Self-similarity of complex networks, *Nature*, *433*, 392–395.

Stouffer, R. J., et al. (2006), GFDL's CM2 global coupled climate models. Part IV: Idealized climate response, *J. Clim.*, *19*, 723–740.

Strogatz, S. H. (2001), Exploring complex networks, *Nature*, *410*, 268–276.

Suarez, M. J., and P. S. Schopf (1998), A delayed action oscillator for ENSO, *J. Atmos. Sci.*, *45*, 549–566.

Swanson, K. L., and A. A. Tsonis (2009), Has the climate recently shifted?, *Geophys. Res. Lett.*, *36*, L06711, doi:10.1029/2008GL037022.

Thompson, D. W. J., and J. M. Wallace (1998), The Arctic Oscillation signature in the wintertime geopotential height and temperature fields, *Geophys. Res. Lett.*, *25*(9), 1297–1300.

Trenberth, K. E., and J. W. Hurrell (1994), Decadal atmospheric-ocean variations in the Pacific, *Clim. Dyn.*, *9*, 303–319.

Tsonis, A. A. (1992), *Chaos: From Theory to Applications*, 274 pp., Plenum, New York.

Tsonis, A. A., and J. B. Elsner (1988), The weather attractor over very short timescales, *Nature*, *33*, 545–547.

Tsonis, A. A., and J. B. Elsner (1989), Chaos, strange attractors and weather, *Bull. Am. Meteorol. Soc.*, *70*, 16–23.

Tsonis, A. A., and J. B. Elsner (1996), Mapping the channels of communication between the tropics and higher latitudes in the atmosphere, *Physica D*, *92*, 237–244.

Tsonis, A. A., and K. L. Swanson (2008), Topology and predictability of El Niño and La Niña networks, *Phys. Rev. Lett.*, *100*, 228502, doi:10.1103/PhysRevLett.100.228502.

Tsonis, A. A., and K. L. Swanson (2011), Climate mode covariability and climate shifts, *Int. J. Bifurcat. Chaos*, *21*, 3549–3556, doi:10.1142/S0218127411030714.

Tsonis, A. A., G. N. Triantafyllou, and J. B. Elsner (1994), Searching for determinism in observed data: A review of the issues involved, *Nonlinear Processes Geophys.*, *1*, 12–25.

Tsonis, A. A., K. L. Swanson, and P. J. Roebber (2006), What do networks have to do with climate?, *Bull. Am. Meteorol. Soc.*, *87*, 585–595, doi:10.1175/BAMS-87-5-585.

Tsonis, A. A., K. Swanson, and S. Kravtsov (2007), A new dynamical mechanism for major climate shifts, *Geophys. Res. Lett.*, *34*, L13705, doi:10.1029/2007GL030288.

Tsonis, A. A., K. L. Swanson, and G. Wang (2008), On the role of atmospheric teleconnection in climate, *J. Clim.*, *21*, 2990–3001.

Tsonis, A. A., G. Wang, K. L. Swanson, F. A. Rodrigues, and L. D. F. Costa (2010), Community structure and dynamics in climate networks, *Clim. Dyn.*, *37*, 933–940, doi:10.1007/s00382-010-0874-3.

Vanassche, P., G. G. E. Gielen, and W. Sansen (2003), Behavioral modeling of (coupled) harmonic oscillators, *IEEE Trans. Comput.-Aided Design Integrated Circuits Syst.*, *22*, 1017–1027.

Verdon, D. C., and S. W. Franks (2006), Long-term behaviour of ENSO: Interactions with the PDO over the past 400 years inferred from paleoclimate records, *Geophys. Res. Lett.*, *33*, L06712, doi:10.1029/2005GL025052.

Vimont, D. J., D. S. Battisti, and A. C. Hirst (2001), Footprinting: A seasonal connection between the tropics and mid-latitudes, *Geophys. Res. Lett.*, *28*, 3923–3926.

Vimont, D. J., J. M. Wallace, and D. S. Battisti (2003), The seasonal footprinting mechanism in the Pacific: Implications for ENSO, *J. Clim.*, *16*, 2668–2675.

Wallace, J. M., and D. S. Gutzler (1981), Teleconnections in the geopotential height field during the Northern Hemisphere winter, *Mon. Weather Rev.*, *109*, 784–812.

Wang, G., K. L. Swanson, and A. A. Tsonis (2009), The pacemaker of major climate shifts, *Geophys. Res. Lett.*, *36*, L07708, doi:10.1029/2008GL036874.

Wang, H., and R. Fu (2000), Influence of ENSO SST anomalies and water storm-tracks on the interannual variability of the upper tropospheric water vapor over the Northern Hemisphere extratropics, *J. Clim.*, *13*, 59–73.

Watts, D. J., and S. H. Strogatz (1998), Collective dynamics of 'small-world' networks, *Nature*, *393*, 440–442.

Webster, P. J., and J. R. Holton (1982), Wave propagation through a zonally varying basic flow: The influences of mid-latitude forcing in the equatorial regions, *J. Atmos. Sci.*, *39*, 722–733.

Wittenberg, A. T., A. Rosati, N.-C. Lau, and J. J. Ploshay (2006), GFDL's CM2 global coupled climate models. Part III: Tropical Pacific climate and ENSO, *J. Clim.*, *19*, 698–722.

Yamasaki, K., A. Gozolchiani, and S. Havlin (2008), Climate networks around the globe are significantly affected by El Niño, *Phys. Rev. Lett.*, *100*, 228501, doi:10.1103/PhysRevLett.100.228501.

Zhang, R., T. L. Delworth, and I. M. Held (2007), Can the Atlantic Ocean drive the observed multidecadal variability in Northern Hemisphere mean temperature?, *Geophys. Res. Lett.*, *34*, L02709, doi:10.1029/2006GL028683.

Zhou, C. S., and J. Kurths (2006), Dynamical weights and enhanced synchronization in adaptive complex networks, *Phys. Rev. Lett.*, *96*, 164102, doi:10.1103/PhysRevLett.96.164102.

A. A. Tsonis, Atmospheric Sciences Group, Department of Mathematical Sciences, University of Wisconsin-Milwaukee, Milwaukee, WI 53201-0413, USA. (aatsonis@uwm.edu)